International Journal of Rotating Machinery
1995, Vol. 2, No. 2, pp. 131-138
Reprints available directly from the publisher
Photocopying permitted by license only

A Numerical Study on Turbulent Couette Flow and Heat Transfer in Concentric Annuli by Means of Reynolds Stress Turbulence Model

SHUICHI TORII
Department of Mechanical Engineering, Kagoshima University, 1-21-40, Korimoto, Kagoshima 890, Japan

WEN-JEI YANG
Department of Mechanical Engineering and Applied Mechanics, The University of Michigan, Ann Arbor, Michigan, 48109, U.S.A.

A numerical study is performed to investigate fluid flow and heat transfer characteristics in a concentric annulus with a slightly heated inner core moving in the flow direction and a stationary, insulated outer cylinder. Emphasis is placed on the effect of inner core movement on the flow structures, i.e. the normal components of the Reynolds stress and its off-diagonal one. A Reynolds stress turbulence model is employed to obtain these turbulence quantities. The governing boundary-layer equations are discretized by means of a control volume finite-difference technique and numerically solved using the marching procedure. It is found from the study that (i) the streamwise movement of the inner core causes an attenuation in the normal Reynolds stresses, although the inherent anisotropy is maintained and the appreciable turbulence remains, (ii) the Reynolds stress in the inner wall region is substantially diminished due to the inner core movement, resulting in a decrease in the heat transfer performance, and (iii) an increase in the velocity ratio of the moving inner core of the fluid flow induces a decrease in the Nusselt number as well as the Reynolds stress in the region near the inner core.

Key Words: *Turbulent Couette Flow; Reynolds Stress Turbulence Model; Numerical Analysis; Finite-Difference Method; Concentric Annulus*

INTRODUCTION

The problems of heat transfer and fluid flow in concentric annuli can be classified three categories: (i) stationary cylinder case, (ii) parallel Couette flow case and (iii) circular Couette flow case. The present study is focused on turbulent transport phenomenon in the parallel Couette flow, which refers to a flow in a concentric annulus with one surface moving in the flow direction and the other remaining stationary (or both surface moving in the flow direction at different velocities).

Barrow and Pope [1987] conducted a simple analysis simulating flow and heat transfer in railway tunnels (such as the 54-km long Seikan tunnel in Japan and the Channel tunnel between England and France). Shigechi et al. [1990] obtained analytical solutions for the friction factor and Nusselt number for turbulent fluid flow and heat transfer in concentric annuli with moving inner cores, using a modified mixing length model, originally proposed by van Driest [1956]. It was disclosed that as the relative velocity (i.e. the velocity ratio of a moving inner core to the fluid flow) is increased, the friction factor is diminished while the Nusselt number is enhanced. The same numerical study was performed by Torii and Yang [1994], who employed the existing k-ϵ turbulence models. It was found that: (i), the streamwise movement of the inner wall causes an attenuation in the turbulent kinetic energy, resulting in a reduction in the heat transfer rate and (ii), an increase in the relative velocity causes a decrease in both the friction factor and the Nusselt number as well as a reduction in the turbulent kinetic energy in the wall inner region. Since the two-equation k-ϵ model basically assumes isotropic turbulence structure, it cannot precisely reproduce the anisotropy of turbulence caused by the inner core moving in the flow direction. In order to obtain the detailed infor-

mation pertinent to the flow structures, the higher order closure model, i.e. a Reynolds stress turbulence model is employed.

Hanjalic and Launder [1976] and Prud'homme and Elghobashi [1986] proposed a low Reynolds number version of a Reynolds stress turbulence model, which can predict turbulence quantities in the vicinity of the wall as well as in the region far from the wall. However, it was found from the preliminary calculation that both models were unable to reproduce the inherent anisotropy in the near-wall region of isothermal circular tube flows. Better accuracy in this region was achieved by the Reynolds stress model of Launder and Shima [1989] based on a full second-momentum closure expressed in terms of the turbulent Reynolds number and independent Reynolds stress invariants.

The purpose of the present study is to investigate turbulent flow and heat transfer characteristics in concentric annuli with the inner core moving in the flow direction. The Reynolds stress turbulence model proposed by Launder and Shima is employed to shed light on the mechanism of the transport phenomena. Emphasis is placed on the effects of core movement on the flow structures, i.e. the three normal components of the Reynolds stress and its off-diagonal one.

GOVERNING EQUATION AND SOLUTION PROCEDURE

Consideration is given to a steady turbulent annular flow in which a slightly heated inner core moves in the flow direction and an insulated outer cylinder is held stationary. The physical configuration and the cylinder coordinate system are shown in Fig. 1. Under the assumptions of constant fluid properties and negligible viscous dissipation, the boundary layer approximation yields the governing equations as:

Continuity equation:

$$\frac{\partial \bar{u}}{\partial x} + \frac{\partial \bar{v}}{\partial r} + \frac{\bar{v}}{r} = 0 \tag{1}$$

Streamwise momentum equation:

$$\bar{u}\frac{\partial \bar{u}}{\partial x} + \bar{v}\frac{\partial \bar{u}}{\partial r} = -\frac{1}{\rho}\frac{d\bar{P}}{dx} + \frac{1}{r}\frac{\partial}{\partial r}(r\nu\frac{\partial \bar{u}}{\partial r} - \overline{ruv}) \tag{2}$$

Energy equation:

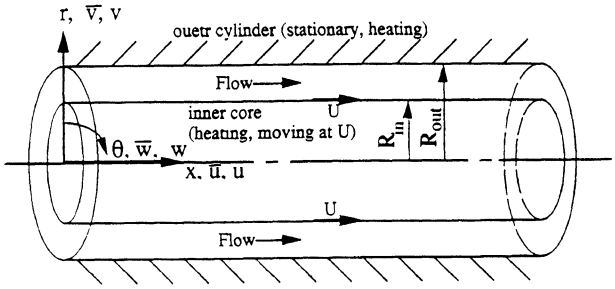

FIGURE 1 Physical system and coordinate.

$$\bar{u}\frac{\partial \bar{T}}{\partial x} + \bar{v}\frac{\partial \bar{T}}{\partial r} = \frac{1}{r}\frac{\partial}{\partial r}(r\alpha\frac{\partial \bar{T}}{\partial r} - \overline{rvt}) \tag{3}$$

A conventional gradient-type diffusion approximation can be employed to express $-\overline{vt}$, as

$$-\overline{vt} = \alpha_t \frac{\partial \bar{T}}{\partial r} \tag{4}$$

The turbulent thermal diffisivity α_t in Eq. (4) is given by

$$\alpha_t = \frac{\nu_t}{Pr_t}, \tag{5}$$

where 0.9 is adapted as the value of Pr_t. The turbulent viscosity ν_t can be represented through Boussinesq's approximation, as

$$\nu_t = \frac{-\overline{uv}}{\frac{\partial \bar{u}}{\partial r}} \tag{6}$$

The Reynolds stress turbulence model proposed by Launder and Shima [1989] is employed to evaluate $-\overline{uv}$ in Eq. (2). The transport equations can be expressed as

$\overline{u^2}$:

$$\bar{u}\frac{\partial \overline{u^2}}{\partial x} + \bar{v}\frac{\partial \overline{u^2}}{\partial r} = \frac{1}{r}\frac{\partial}{\partial r}\{r(\mu + C_s\frac{k}{\epsilon}\overline{v^2})\frac{\partial \overline{u^2}}{\partial r}\}$$
$$-2(1-f_2)\overline{uv}\frac{\partial \bar{u}}{\partial r} - \frac{2}{3}f_2\overline{uv}\frac{\partial \bar{u}}{\partial r}f_1\overline{u^2}\frac{\epsilon}{k}$$
$$+\frac{2}{3}(f_1 - 1)\epsilon + f_{1w}f_x\overline{v^2}\frac{\epsilon}{k} - \frac{2}{3}f_{2w}f_x\overline{uv}\frac{\partial \bar{u}}{\partial r} \tag{7}$$

$\overline{v^2}$:

$$-u\frac{\partial\overline{v^2}}{\partial x}+v\frac{-\partial\overline{v^2}}{\partial r}=\frac{1}{r}\frac{\partial}{\partial r}\left\{r(\mu+C_s\frac{k}{\epsilon}\overline{v^2})\frac{\partial\overline{v^2}}{\partial r}\right\}$$
$$-2(\nu+C_s\overline{w^2}\frac{k}{\epsilon})\frac{\overline{v^2}-\overline{w^2}}{r^2}-\frac{2}{3}f_2\overline{uv}\frac{\partial\bar{u}}{\partial r}f_1\overline{v^2}\frac{\epsilon}{k}$$
$$+\frac{2}{3}(f_1-1)\epsilon-2f_{1w}f_x\overline{v^2}\frac{\epsilon}{k}+\frac{4}{3}f_{2w}f_x\overline{uv}\frac{\partial\bar{u}}{\partial r} \quad (8)$$

$\overline{w^2}$:

$$-u\frac{\partial\overline{w^2}}{\partial x}+v\frac{-\partial\overline{w^2}}{\partial r}=\frac{1}{r}\frac{\partial}{\partial r}\left\{r(\mu+C_s\frac{k}{\epsilon}\overline{v^2})\frac{\partial\overline{w^2}}{\partial r}\right\}$$
$$+2(\nu+C_s\overline{w^2}\frac{k}{\epsilon})\frac{\overline{v^2}-\overline{w^2}}{r^2}-\frac{2}{3}f_2\overline{uv}\frac{\partial\bar{u}}{\partial r}f_1\overline{w^2}\frac{\epsilon}{k}$$
$$+\frac{2}{3}(f_1-1)\epsilon+f_{1w}f_x\overline{v^2}\frac{\epsilon}{k}-\frac{2}{3}f_{2w}f_x\overline{uv}\frac{\partial\bar{u}}{\partial r} \quad (9)$$

$\overline{uv}$:

$$-u\frac{\partial\overline{uv}}{\partial x}+v\frac{-\partial\overline{uv}}{\partial r}=\frac{1}{r}\frac{\partial}{\partial r}\left\{r(\mu+C_s\frac{k}{\epsilon}\overline{v^2})\frac{\partial\overline{uv}}{\partial r}\right\}$$
$$-(\nu+C_s\overline{w^2}\frac{k}{\epsilon})\frac{\overline{uv}}{r^2}-(1-f_2)\overline{v^2}\frac{\partial\bar{u}}{\partial r}f_1\overline{uv}\frac{\epsilon}{k}$$
$$-\frac{3}{2}f_{1w}f_x\overline{uv}\frac{\epsilon}{k}-\frac{3}{2}f_{2w}f_x\overline{v^2}\frac{\partial\bar{u}}{\partial r} \quad (10)$$

Turbulent energy dissipation rate is determined from

$$-u\frac{\partial\epsilon}{\partial x}+v\frac{-\partial\epsilon}{\partial r}=\frac{1}{r}\frac{\partial}{\partial r}\left\{r(\mu+C_s\frac{k}{\epsilon}\overline{v^2})\frac{\partial\epsilon}{\partial r}\right\}$$
$$+(C_{\epsilon1}+\varphi_1+\varphi_2)\overline{uv}\frac{\epsilon}{k}\frac{\partial\bar{u}}{\partial r}$$
$$-C_{\epsilon2}\frac{\epsilon}{k}\left\{\epsilon-2\nu\left(\frac{\partial\sqrt{k}}{\partial r}\right)^2\right\} \quad (11)$$

The empirical constants and model functions in Eqs. (7), (8), (9), (10) and (11) are summarized in Table 1.

The governing equations are subject to the following boundary conditions:

x = 0 (start of heating): hydrodynamically fully developed annular flow without an inner core movement

TABLE 1
Empirical constants and functions for a Reynolds stress turbulence model.

C_1	2.58	C_2	0.75	C_{1w}	1.67	C_{2w}	0.5	C_1	2.5
C_s	0.22	C_ϵ	0.18	$C_{\epsilon1}$	1.45	$C_{\epsilon2}$	1.9		
A_2	$\left(\frac{\overline{u^2}}{k}-\frac{2}{3}\right)^2+\left(\frac{\overline{v^2}}{k}-\frac{2}{3}\right)^2+\left(\frac{\overline{w^2}}{k}-\frac{2}{3}\right)^2+2\left(\frac{\overline{uv}}{k}\right)^2$								
A_3	$\left(\frac{\overline{u^2}}{k}-\frac{2}{3}\right)^3+\left(\frac{\overline{v^2}}{k}-\frac{2}{3}\right)^3+\left(\frac{\overline{w^2}}{k}-\frac{2}{3}\right)^3+3\left(\frac{\overline{uv}}{k}\right)^2\left\{\left(\frac{\overline{u^2}}{k}-\frac{2}{3}\right)+\left(\frac{\overline{v^2}}{k}-\frac{2}{3}\right)\right\}$								
A	$1-\frac{9}{8}A_2+\frac{9}{8}A_3$								
f_x	$\frac{k^{3/2}}{C_1y\epsilon}$								
f_{R1}	$1-\exp\{-(0.0067R_t)^2\}$								
f_{R2}	$\exp\{-(0.002R_t)^{1/2}\}$								
f_1	$1+C_1f_{R1}AA_2^{1/4}$								
f_2	$C_2A^{1/2}$								
f_{1w}	$-\frac{2}{3}f_1+C_{1w}$								
f_{2w}	$\frac{1}{2}\left\{\frac{2}{3}(f_2-1)+C_{2w}+\left\lvert\frac{2}{3}(f_2-1)+C_{2w}\right\rvert\right\}$								
ψ_1	$1.5A(-\frac{\overline{uv}}{\epsilon}\frac{\partial\bar{u}}{\partial r}-1)$								
ψ_2	$0.35f_{R2}(1-0.3A_2)$								

r = R_{in} (inner wall): $\bar{u} = U$ (velocity of a inner cylinder), $\overline{u^2} = \overline{v^2} = \overline{w^2} = \overline{uv} = \epsilon = 0$.

$$-\frac{\partial \bar{T}}{\partial r} = \frac{q_w}{\lambda_w}$$

r = R_{out} (outer wall): $\bar{u} = \overline{u^2} = \overline{v^2} = \overline{w^2} = \overline{uv} = \epsilon = 0$,

$$\frac{\partial \bar{T}}{\partial r} = 0 \text{ (insulation)}$$

The governing equations are discretized by means of a control volume method [1980]. Since all turbulence quantities as well as the time-averaged streamwise velocity vary rapidly in the near-wall region, nonuniform cross-stream grids are used in which the size is increased in a geometric ratio with the maximum size being kept within 3 % of the hydrodynamic radius. The number of typical control volumes used in the radial direction are 45 at Re = 10,000 and 52 at 46,000. In order to ensure the accuracy of calculated results, at least two control volumes are always located in the viscous sublayer. The resulting equations are solved from the inlet proceeding in the downstream direction by means of the marching procedure, because the equations are parabolic. The axial control volume size is constant and five times the minimum radial size at the wall. At each axial location, the pressure gradient $d\bar{P}/dx$ in Eq. (2) is corrected at every iteration to conserve the total mass flow rate. The procedure is repeated until a convergence criterion is satisfied. In the present study, it is set at

$$\text{maximum}\left[\frac{\phi^M - \phi^{M-1}}{\phi^{M-1}_{max}}\right] < 1 \times 10^{-4} \qquad (12)$$

for all the variables ϕ ($\bar{u}$, $\overline{u^2}$, $\overline{v^2}$, $\overline{w^2}$, $\overline{uv}$, $\bar{T}$, and ϵ). The superscripts M and M − 1 in Eq. (12) indicate two successive iterations, while the subscript "max" refers to a maximum value over the entire fields of iterations. Throughout numerical calculations, the number of control volumes is properly selected between 45 and 92 to ensure validation of the numerical procedures and to obtain grid-independent solutions. It results in no appreciable difference between the numerical results with different grid spacing. The calculation conditions are summarized in Table 2, including the Reynolds number, wall heat flux, relative velocity and tube size.

It is necessary to verify both the turbulence model employed here and the reliability of the computer code by comparing numerical predictions with experimental results for the flow fields. The model is applied to a flow in an annulus with a stationary, slightly heated inner core. Numerical results for the streamwise velocity, three components of Reynolds stress, its off-diagonal one and Nusselt number are obtained at a location 200 tube diameter downstream from the inlet, where thermally and hydrodynamically developed flow is realized. The experimental data of Brighton and Jones [1964] are used for comparison. Figure 2 depicts the radial distributions of the time-averaged streamwise velocity (dimensionless velocity u^+ versus y^+) at Re = 46,000. Figure 2(a) and (b) correspond to the distributions from the inner and outer walls to the location of the maximum stremwise velocity, respectively. It is observed that the model yields a better agreement with the experimental data, and predict the velocity profile with well-known characteristics of the logarithmic region, i.e. the universal wall law. Figure 3 shows the radial distributions of three normal components of the Reynolds stress tensor at Re = 46,000. The numerical results are normalized by the friction velocity, u^*_{out}, on the outer wall. The model predicts an inherent anisotropy of the annular flow, although its accuracy is somewhat inferior near the inner and outer walls than in the center region. Figure 4 illustrates the radial distribution of the calculated Reynolds stress at Re = 46,000. The ordinate in the figure is normalized by the square of the friction velocity $(u^*_{out})^2$ on the outer wall. The predicted results are in good agreement with the experimental data. Figure 5 present both the Nusselt number and the friction factor as a

TABLE 2.
Calculation conditions.

Fluid	R_{in}/R_{out}	q_w (W/m^2)	Re	U*
			10000	
			20000	
			30000	0.0
	0.50		40000	
Air		1000	50000	0.5
	0.56		60000	
			70000	1.0
			80000	
			90000	
			100000	

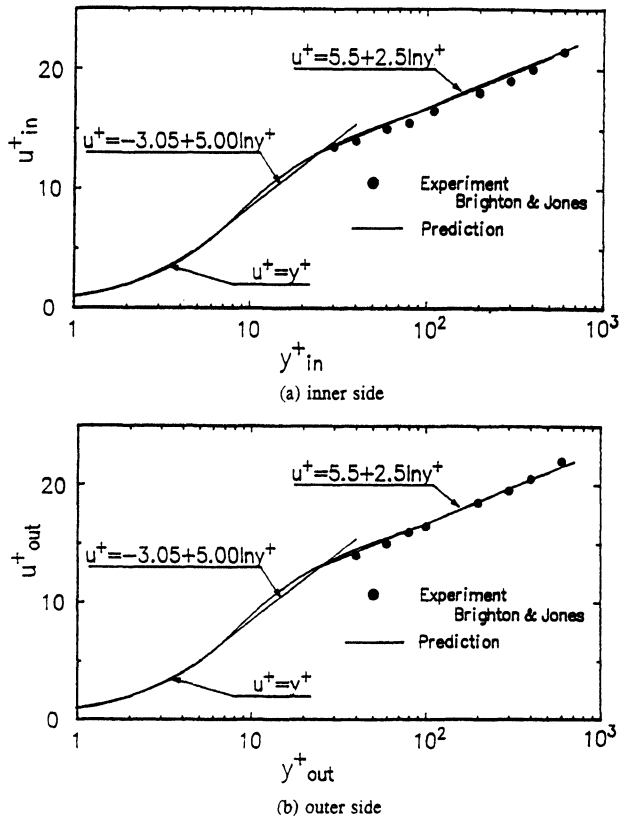

FIGURE 2 Distribution of predicted time-averaged streamwise velocity in a stationary concentric annulus for Re = 46,000 and R_{in}/R_{out} = 0.56, (a) inner side and (b) outer side.

function of the Reynolds number. Dalle Donne andMeerwald [1966] derived the following correlations for the Nusselt number and friction factor at the inner wall of the annulus as

$$Nu = 0.0181\left(\frac{R_{out}}{R_{in}}\right)^{0.2} Re^{0.8} Pr^{0.4} \left(\frac{\overline{T}_{win}}{T_{inlet}}\right)^{-0.18} \quad (13)$$

and

$$f = 0.0615\left(\frac{R_{out}/R_{in} - 1}{R_{out}/R_{in}}\right)^{0.1} Re^{-0.22} \quad (14)$$

respectively. The two equations are superimposed in Fig. 5 as solid straight lines. Note that Fig. 5 is under the temperature ratio of the inner wall to the inlet fluid, $\overline{T}_{win}/\overline{T}_{inlet}$, of unity, and the radial ratio, R_{in}/R_{out}, of 0.56. The calculated Nusselt number and friction factor are in good agreement with the correlations, Eqs. (13) and (14). The validity of the computer code and the accuracy for the model employed here are thus confirmed.

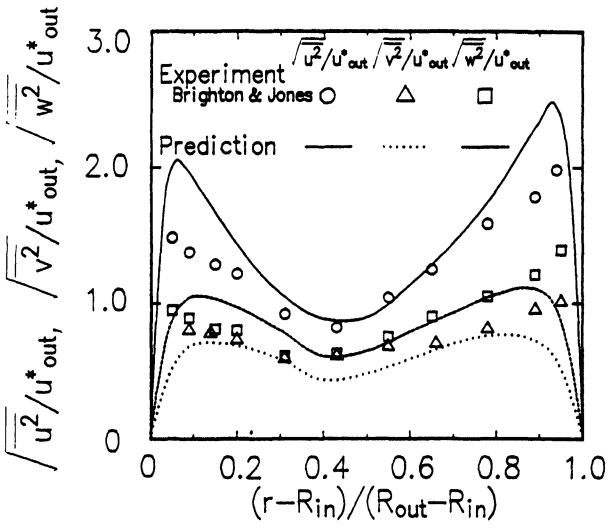

FIGURE 3 Radial distribution of predicted normal Reynolds stresses in a stationary concentric annulus for Re = 46,000 and R_{in}/R_{out} = 0.56.

NUMERICAL RESULTS AND DISCUSSION

Numerical results of the Nusselt number are illustrated in Fig. 6 with the velocity ratio of a moving inner core to a fluid flow, U*, as the parameter. It is observed that the Nusselt number diminishes with an increase in the dimensionless relative velocity. A similar trend is reported by Torii and Yang [1994], who employ the existing k-ϵ turbulence models. It is disclosed that the substantial reduction in the Nusselt number is attributed to the inner core movement in the flow direction.

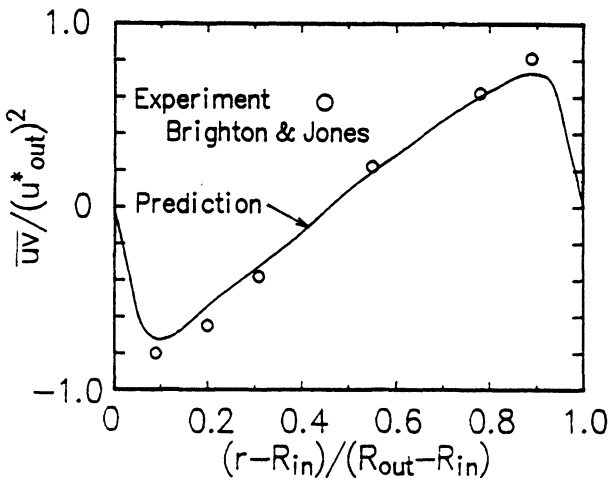

FIGURE 4 Radial distribution of predicted Reynolds stress in a stationary concentric annulus for Re = 46,000 and R_{in}/R_{out} = 0.56.

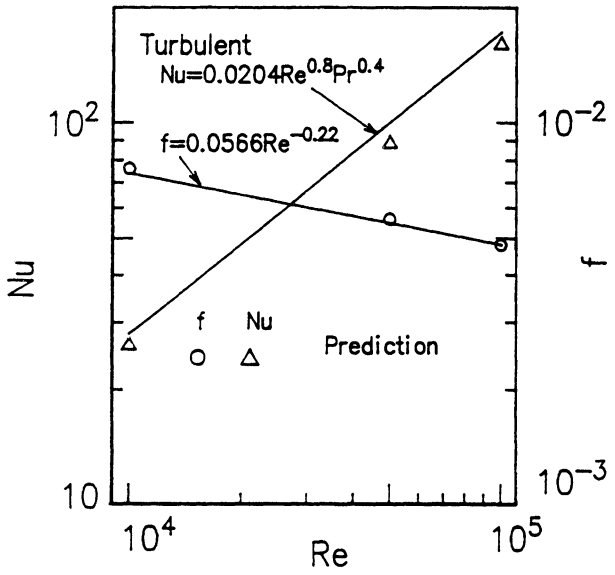

FIGURE 5 Predicted Nusselt number and friction factor in a stationary concentric annulus for R_{in}/R_{out} = 0.56 and x/D = 200.

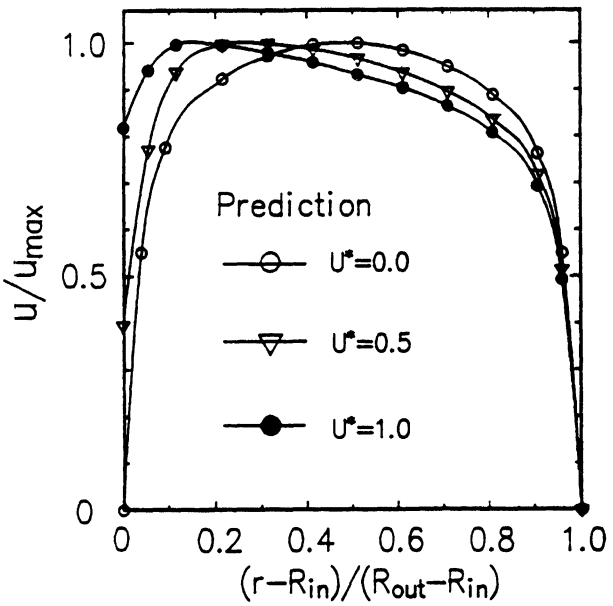

FIGURE 7 Variation of time-averaged streamwise velocity profiles with dimensionless relative velocity for Re = 50,000 and R_{in}/R_{out} = 0.5.

Numerical results for the streamwise velocity, three normal components of the Reynolds stress and its off-diagonal one at Re = 50,000 are calculated in order to explore the mechanisms of turbulent parallel Couette flows in an annulus. Figure 7 depicts the radial profiles of the time-averaged streamwise velocity $\bar{u}/\bar{u}_{max}$ for different values of the dimensionless relative velocity, U*. It is obtained that as U* is increased, the peak of $\bar{u}/\bar{u}_{max}$ shifts toward the inner side, resulting in a substantial deformation in the velocity profile of the fully-developed turbulent annular flow with a stationary inner core. This implies that the velocity gradient at the inner wall is significantly reduced by the streamwise movement of the inner core, while only a slight change occurs in the outer wall region. The radial profiles of three normal components of the Reynolds stress are illustrated in Fig. 8 at different dimensionless relative velocities. One observes that (i) the three normal stress levels in the inner wall region are substantially reduced with an increase in U*, although the inherent anisotropy is maintained and the appreciable turbulence remains, and (ii) only a slight effect appears in the outer wall side. The corresponding variation of the Reynolds stress with a change in U* is shown in Fig. 9. The Reynolds stress level in the inner wall region is diminished with an increase in U*, and almost disappears at U* = 1.0. In contrast, the Reynolds stress in the center region increases, while no effect appears in the vicinity of the outer wall. This behavior is in accord with the variation of the streamwise velocity, $\bar{u}/\bar{u}_{max}$, in Fig. 7. Since the eddy diffisivity concept is employed to determine the turbulent heat flux $-\overline{vt}$, it is directly related to the Reynolds stress through Eqs. (4), (5) and (6). Hence, a reduction in the Reynolds stress is ascribed to an attenuation in the Nusselt number, as observed in Fig. 6.

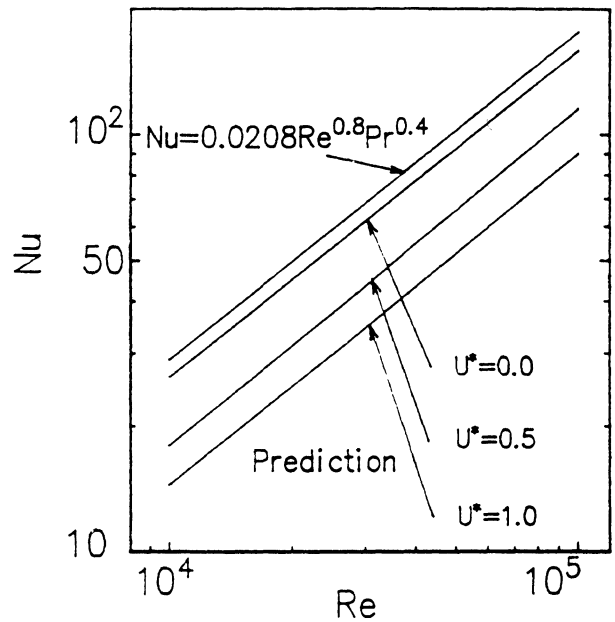

FIGURE 6 Variation of predicted Nusselt numbers with dimensionless relative velocity for R_{in}/R_{out} = 0.5 and x/D = 200.

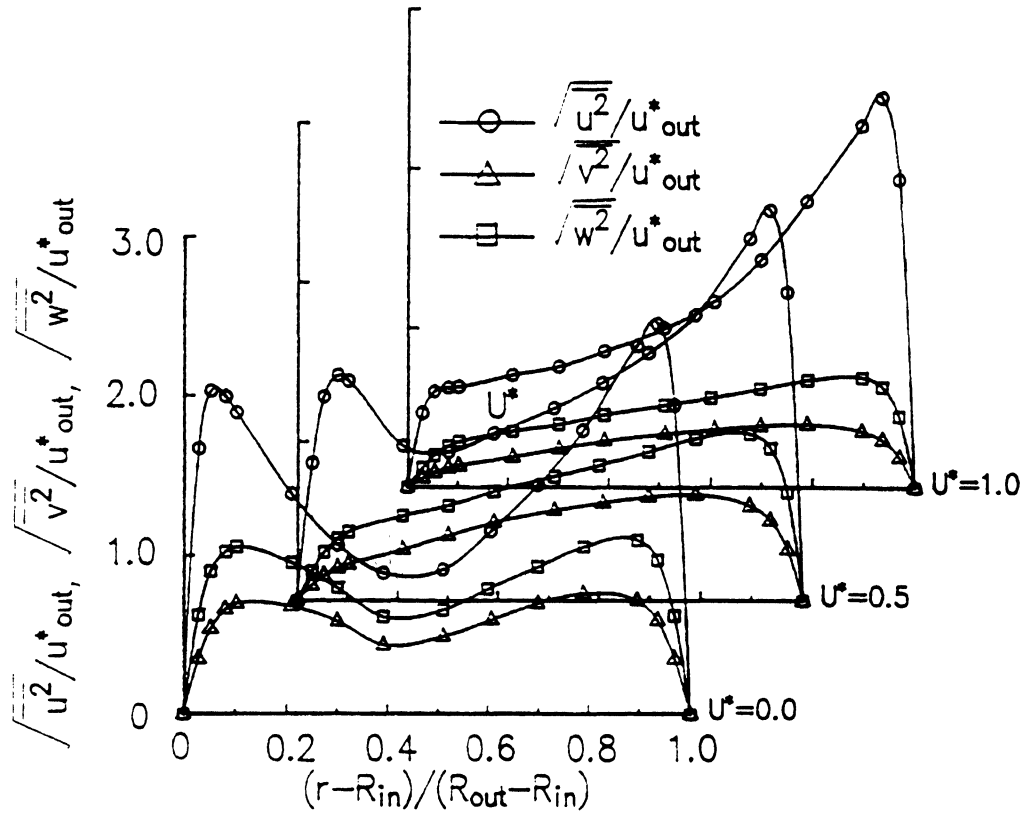

FIGURE 8 Variation of normal components of Reynolds stress with dimensionless relative velocity for Re = 50,000 and R_{in}/R_{out} = 0.5.

In summary, a decrease in the Nusselt number, as seen in Fig. 6, is caused by the streamwise movement of the inner core. This trend is amplified with an increase in the relative velocity. The mechanism is that: in the region near the inner core, a reduction in the velocity gradient induced by its streamwise movement suppresses the Reynolds stress, resulting in a decrease in the heat transfer performance.

SUMMARY

A Reynolds stress turbulence model by Launder and Shima has employed to investigate transport phenomena in concentric annulus with a slightly heated inner core moving in the flow direction. Consideration is given to the influence of relative velocity on the flow structure. The results are summarized as follows:

A Reynolds stress turbulence model predicts a reduction in the Nusselt number with an increase in the relative velocity. It is also disclosed that: (i) an inner core movement causes a decrease in the velocity gradient at the inner wall, a substantial deformation of the velocity profile and an attenuation in the three normal components of the Reynolds stress in the inner wall, and (i) however, an appreciable turbulence remains and its inherent anisotropy is maintained. Consequently, the streamwise movement of the inner core suppresses the

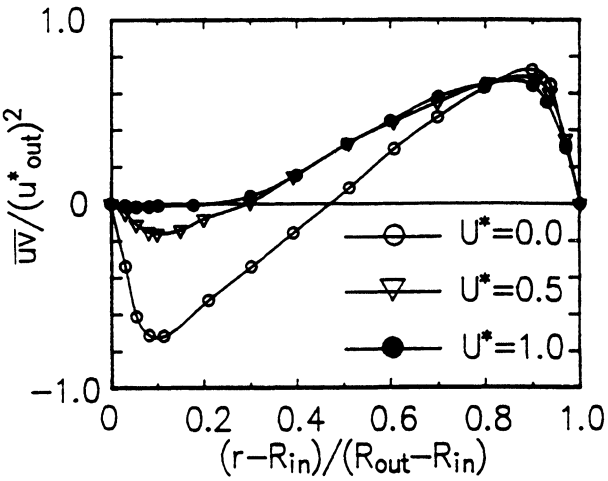

FIGURE 9 Variation of Reynolds stress profiles with dimensionless relative velocity for Re = 50,000 and R_{in}/R_{out} = 0.5.

Reynolds stress in the vicinity of the inner wall, resulting in the deterioration of heat transfer performance.

Nomenclature

D	hydraulic diameter of the annulus, $2(R_{out} - R_{in})$, m
f	friction factor
h	heat transfer coefficient, W/m^2K
k	turbulent kinetic energy, $(\overline{u^2} + \overline{v^2} + \overline{w^2})/2$, m^2/s^2
Nu	Nusselt number, hu_m/λ
P	time-averaged pressure, Pa
Pr	Prandtl number
Pr_t	turbulent Prandtl number
q	heat flux, W/m^2
r	radial coordinate, m
Re	Reynolds number, u_mD/ν
R_{in}	inner radius of the annulus, m
R_{out}	outer radius of the annulus, m
R_t	turbulent Reynolds number, $k^2/\epsilon\nu$
T	time-averaged temperature, K
t	fluctuating temperature component, K
U	velocity of a moving inner cylinder, m/s
U^*	dimensionless relative velocity, U/u_m
u_m	axial mean velocity over tube cross section, m/s
$\bar{u}, \bar{v}, \bar{w}$	time-averaged velocity components in axial, radial and tangential directions, respectively m/s
u, v, w	fluctuating velocity components in axial, radial and tangential directions, respectively m/s
u^*	friction velocity, m/s
u^+	dimensionless velocity, $\bar{u}/u^*$
$-\overline{uv}$	Reynolds stress, m^2/s^2
$-\overline{vt}$	turbulent heat flux, mK/s
x	axial coordinate, m
y	distance from wall, m
y^+	dimensionless distance, u^*y/ν
α, α_t	molecular and turbulent thermal diffusivities, m^2/s
ϵ	turbulent energy dissipation rate, m^2/s^3
λ	molecular thermal conductivity, W/mK
ν, ν_t	molecular and turbulent viscosities, m^2/s
$\sigma_k, \sigma_\epsilon$	turbulent Prandtl numbers for k and ϵ, respectively

Subscripts

in	inner side
inlet	inlet
max	maximum
out	outer side
w	wall

Superscripts

$\bar{}$	time-averaged value

References

Barrow, H., and Pope, C. W., 1987. A Simple Analysis of Flow and Heat Transfer in Railway Tunnels, *Heat Fluid Flow*, Vol. 8, pp. 119–123.

Brighton, J., and Jones, J. B., 1964. Fully Developed Turbulent Flow in Annuli, *Trans. ASME*, Ser. D, pp. 835–844.

Dalle Donne, M., and Meerwald, E., 1966. Experimental Local Heat Transfer and Average Friction Coefficients for Subsonic Turbulent Flow of Air in an Annulus at High Temperature, *Int. J. Heat Mass Transfer*, Vol. 9, pp. 1361–1376.

Hanjalic, K., and Launder, B. E., 1976. Contribution towards a Reynolds-Stress Closure for Low-Reynolds-Number Turbulence, *J. Fluid Mech.*, Vol. 74, no. 4, pp. 593–610.

Launder, B. E. and Shima, N., 1989. Second-Momentum Closure for the Near-Wall Sublayer: Development and Application, *AIAA J.*, Vol. 27, no. 10, pp. 1319–1325.

Patankar, S. V., 1980. *Numerical Heat Transfer and Fluid Flow*, Hemisphere, Washington, DC.

Prud'homme, M., and Elghobashi, S., 1986. Turbulent Heat Transfer near the Reattachment of Flow Downstream of a Sudden Pipe Expansion, *Numerical Heat Transfer*, Vol. 10, pp. 349–368.

Torii, S., and Yang, W. J., 1994. A Numerical Study on Turbulent Couette Flow and Heat Transfer in Concentric Annuli, *Int. J. Numerical Methods for Heat & Fluid Flow*, Vol. 4, pp. 367–377.

van Driest, E. R., 1956. On Turbulent Flow near a Wall, *J. Aerosp. Sci.*, Vol. 23, pp. 1007–1011.